Electric Power Systems Research 229 (2024) 110056

Contents lists available at ScienceDirect

Electric Power Systems Research

journal homepage: www.elsevier.com/locate/epsr

Reactive power control of micro-grids using FOSMC for grid code compliance during asymmetrical voltage sags

Reza Deihimi Kordkandi [a], Mehrdad Tarafdar Hagh [a], Sam Roozbehani [b], Mojtaba Feyzi [c], Navid Bayati [d,*], Thomas Ebel [d]

[a] Faculty of Electrical and Computer Engineering, University of Tabriz, Tabriz, Iran
[b] Renewable Power Generation Research Group, ACECR, Khajeh Nasir Toosi University of Technology Branch, Tehran, Iran
[c] Department of Electrical Engineering, K. N. Toosi University of Technology, Tehran, Iran
[d] Centre for Industrial Electronics, Department of Mechanical and Electrical Engineering, University of Southern Denmark, Sønderborg, Denmark

ARTICLE INFO

Keywords:
Asymmetrical voltage sags
Four-wire system
Fractional-order SMC
LVRT
Micro-grid
Reactive power-sharing

ABSTRACT

Application of micro-grids (MGs) as a solution for future energy systems are significantly increasing in recent years. On the other hand, more stringent requirements are added to grid codes (GCs) of low-voltage distribution networks. Accordingly, this paper proposes a low-voltage ride-through (LVRT) control scheme for four-wire multi-source MGs. The novel strategy is composed of two layers for controlling each phase of the grid-connected sources independently. The primary layer contains a reverse-droop function for each phase and fractional-order sliding-mode-control (FOSMC). The secondary layer determines the total requested reactive power for each phase during symmetrical and asymmetrical voltage drops. Then, the mentioned power is shared among the phases of each inverter based on the reactive power-sharing strategy and GC requirements. Based on the proposed grid-following controller, the voltage of faulty phases is compensated by reactive power injection. In addition, power quality indexes are kept in acceptable ranges during abnormalities, and the FOSMC performs better than the conventional methods. The effectiveness of the proposed scheme is verified through offline simulations in MATLAB/Simulink as well as validation by real-time results.

1. Introduction

1.1. Background

The utilization of small-scale distributed energy resources (DERs) in low and medium-voltage networks is increasing, and as a result, their sudden and collective disconnection from the power system might cause voltage collapse on the grid during severe voltage perturbations. Therefore, the severe impact of the DERs cannot be ignored since their contribution to the power supply is considerable. Thus, the incremental usage of DER systems has become leverage for setting new requirements for power systems. These regulations are called grid codes (GCs), which vary from country to country and cover some grid-connected power sources such as wind turbines and photovoltaic (PV) systems [1]. The mentioned regulations force the sources to stay connected to the main grid during temporary voltage sags and support it by injecting reactive current. An essential requirement of the GC, which has gained much attraction in recent studies, is the low-voltage ride-through (LVRT) capability of the distributed generators (DGs). LVRT curves of the German and Danish GCs are highlighted in Fig. 1a [2]. Besides, in Fig. 1b amount of the reactive power injection per voltage drop is depicted for different scenarios [3]. Most studies cover symmetrical voltage disturbances that only include a minor percentage of the faults such as [4,5], etc. However, asymmetrical faults such as single-phase short-circuits are more probable with an 85 % occurrence rate [6]. In most cases, the conventional three-phase control methods for compensating voltage drops are not applicable for asymmetrical faults since they might affect the operation of safe phases by deteriorating voltage imbalance. Also, reactive power-sharing and reference power tracking in multi-source MGs are important operation factors, which has not been addressed sufficiently in previous studies.

1.2. Literature review

Overall, the solutions in this literature can be divided into three main groups: the methods based on using some types of equipment, grid-forming-based controllers, and grid-following-based strategies, which

* Corresponding author.
E-mail address: navib@sdu.dk (N. Bayati).

https://doi.org/10.1016/j.epsr.2023.110056
Received 15 May 2023; Received in revised form 9 November 2023; Accepted 30 November 2023
Available online 5 January 2024

Nomenclature

Indices

I	Denotes the *i*th inverter of the micro grid
J	Denotes the phase ($j = a, b, or\ c$)
α	Denotes the fractional order of the FOSMC
+-0	Theses superscripts denote the positive, negative and zero sequence of a variable
dq0	These subscripts denote the *d*,*q*, and *0* components of a variable in the synchronous reference frame
Ref	Denotes the reference value of a variable
PQ	These subscripts denote the active and reactive current of the phases

Parameters

R,L,C	Filters of the inverters
Z_{1to4}	Impedance between the DGs and the PCC
Z_{grid}	Impedance between PCC and the main grid
Z_n^i	Impedance of the DGs' Fourth wire
C_1 and C_2	Capacitance of the fourth leg
V_{DC}	Nominal DC voltage of the inverters
V_{AC}	Nominal AC voltage of the grid
V_{rated}	Nominal phase to ground voltage
f_{rated}	Rated frequency of the MG
$S_{rated,i}$	Rated power of DG*i*
$S_{rated,MG}$	Rated power of MG
$m_{p,i}^j$	*P*–*f* slope of the reverse droop
$n_{q,i}^j$	*Q*–*V* slope of the reverse droop
K	Voltage compensation rate
$k_{dq}^{\pm}$	Switching gain of the FOSMC
$C_{dq}^{\pm}$	Gain of the *D* operator in FOSMC
N	estimation order
ω_b, ω_h	Lower and higher frequencies in fractional order transfer function estimation

Variables

P_0^i and Q_0^i	Denotes the constant active and reactive power injected by *i*th DG
f_i	Frequency of *i*th DG
V_i^j	Voltage of phase *j* in DG *i*
$P_{rev,i}^j$, $Q_{rev,i}^j$	Active and reactive power of reverse droop control in phase *j* and DG *i*
$P_{ref,i}^j$, $Q_{ref,i}^j$	Active and reactive power reference of phase *j* in DG *i*
$i_{ref,P,i}^j$, $i_{ref,Q,i}^j$	Active and reactive reference current of phase *j* in DG *i*
$i_{dq,ref}^{\pm}$, $i_{dq}^{\pm}$	Positive and negative sequence of reference and measured current in the d and q component
$V_{dq}^{\pm}$	Positive and negative sequence of measured voltage in the *d* and *q* component
$Sw_{dq}^{\pm}$	Switching states of the inverters which can adopt 0 or 1
$\Delta_{dq}^{\pm}$	Filter uncertainties
$S_{dq}^{\pm}$	Sliding surface of positive and negative sequences in the *d* and *q* coordinates
$v_{dq,ref}^{\pm}$	Reference switching signals of the inverters
$v_s^{dq\pm}$	Switching function of the reference signals
$v_{dq,eq}^{\pm}$	Equivalent values of the reference switching signals
$Q_{add,T}^j$	Total additional reactive power of phase *j* in the MG
$Q_{add,i}^j$	Additional reactive power of phase *j* in DG *i*
$Q_{req,T}^j$	Total requested reactive power from phase *j* of the MG
$S_{empty,i}^j$	Empty capacity of DG *i* in phase *j*.
$P_{ref,i}^j$,$Q_{ref,i}^j$	Active and reactive power reference of phase *j* in DG *i*

are reviewed respectively in the following paragraphs [5].

In the first category, additional hardware such as superconducting magnetic energy storage (SMES) [7] or Battery-Energy-Storage-System (BESS) [8] is utilized for enhancing the LVRT capability of MGs. Although using D-FACTS like D-STATCOM [9] or utilizing superconducting fault current limiters (SFCL) [10,11] and dynamic voltage restorers (DVR) [12] have a considerable impact on the LVRT capability improvement of the MGs, the mentioned equipment is not affordable and requires complicated control methods. Furthermore, only symmetrical faults were studied in most of those works.

Instead of using hardware-dependent schemes, LVRT conditions can be tackled by implementing proper controllers such as the grid-forming-based methods [13,14], which are mainly used for isolated power networks. However, they can be implemented in the grid-tied MGs. Furthermore, conventional and improved direct-droop are commonly used in the grid-forming-based approaches. For example, authors in [15] have presented a control scheme using direct-droop control to fulfill GC

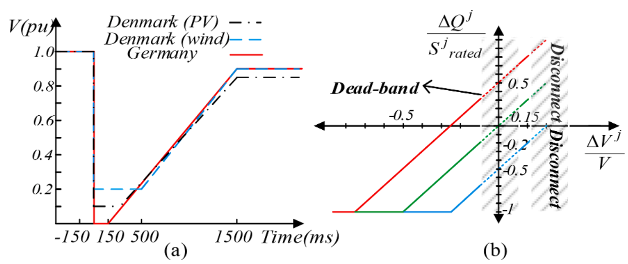

Fig. 1. (a) LVRT curves of Germany and Denmark; (b) Reactive power injection during Voltage sag.

requirements and prevent high currents during faults. Although a particular amount of reactive power has been injected, voltage compensation is not reported in the inverter terminals of the test system. Furthermore, a negative sequence droop-based controller is proposed in [16] to deal with asymmetrical disturbances in MG. Though, the existence of a reactive power-sharing strategy in the presented control scheme seems necessary. Because of this issue, the capacity of the inverters and their parameters in the test system was adopted equally. Also, the droop methods used in the MGs can be mixed with other controllers such as passivity-based-switching functions [17] and fuzzy logic [18,19] to improve the sustainability of the MG against voltage disturbances whereas, these studies could use coordinating strategy between the sources. To fix the aforementioned drawbacks, authors in [20] have presented an LVRT scheme based on the direct-droop method with two control layers. The suggested method is according to independent control of each phase, which can tackle the asymmetrical disturbances. Nevertheless, the reactive power outputs of the inverters were beyond their set-point values and rated capacity, which might be originated from the grid-forming method used in the presented scheme [21].

On the other hand, grid-following-based methods are mainly used for grid-tied MGs and sources [13]. These methods often utilize GC requirements to tackle the voltage drop originating from the upstream grid. For example, authors of [2,22] have used German GC requirements to generate power set-points for inverters. In [2], the injected reactive currents of DGs during asymmetrical faults are balanced, which might pose voltage swell in safe phases. Moreover, in [23,24], a control method based on positive and negative sequences is presented for a single inverter rather than designing a thorough control scheme for multi-source MG. Also, the voltage drop is considered very low in some

Table 1
Literature review describing upsides, downsides, and methodology of each paper.

Control Strategy	Brief description of the implemented methodology	Benefits	drawbacks	Reference
Hardware Dependent strategies	Using an SMES with fault current limiting function	✓ Alleviation of fault current ✓ Decreasing power fluctuation of wind turbine	× Lack of voltage compensation of busses × High cost	[7]
	Using BESS for voltage restoration	✓ Voltage compensation	× High cost × Lack of asymmetrical voltage sag analysis	[8]
	Using D-STATCOM	✓ Voltage Compensation	× Lack of coordinating strategy for reactive power injection	[9]
	Using SFCL and DVR for comparison	✓ Voltage Compensation by 57% using SFCL ✓ Voltage Compensation by 100% using DVR	× High cost × Needing complicated control system × Lack of asymmetrical voltage sag analysis	[10]
	Using an SFCL	✓ PCC voltage improvement to 43.8% of the nominal value	× Voltage has not completely compensated. × Lack of asymmetrical voltage sag analysis	[11]
	Using a DVR	✓ Voltage Compensation by 100% using DVR	× Lack of asymmetrical voltage sag analysis	[12]
Grid-Forming-based strategies	Using improved direct droop controller which is based on P_V and Q_-W functions	✓ Limiting the current during voltage sag occurrence	× The test system is single-source × Lack of any voltage compensation report	[15]
	Using hierarchal two-layer control based on positive- and negative-sequence of droop	✓ Voltage sag compensation	× Discussion lack about LVRT capability of multi-source MGs × Slow response of the presented control	[16]
	Droop method and Passivity-Based-Switching-Function	✓ Effective dynamic response and improving stability margin	× Lack of coordinating strategy between the sources	[17]
	Using hierarchal three-layer control including droop method and Fuzzy-Logic	✓ Improving stability margin of the MG ✓ Reducing resonance effects caused by voltage control	× No report regarding voltage compensation × No report regarding reactive power injection for improving LVRT capability	[18], [19]
	Using improved droop method and independent control of each phase	✓ Voltage compensation during sags ✓ Voltage imbalance factor reduction	× Excessive injection of reactive power × Slow dynamic response	[20]
	Presenting a two-layer scheme including droop and bridge-type fault current limiter	✓ Voltage compensation	× No strategy for asymmetrical voltage sags × No strategy for sharing reactive current in case of multi-source MGs	[21]
Grid-Following-based strategies	Using negative sequence control units alongside German GC reactive power support strategy	✓ Realizing FRT requirements of German and Danish GCs	× Injecting symmetrical current during asymmetrical voltage sags, which can cause voltage swell in safe phases	[2]
	• units German GC reactive power support strategy • Presenting a coefficient for controlling positive- and negative-sequences of the current • Implementing Proportional Resonant control	✓ Compensation of voltage sag ✓ Limiting line current	× High power fluctuation	[22]
	Presenting a coefficient for controlling positive- and negative-sequences of the current	✓ Reducing imbalance factor of the voltage during asymmetrical faults	× Determining reactive power reference offline × Lack of coordinating strategy for reactive power injection	[23], [25]
	Applying the presented coefficient of [22][24]	✓ Limiting fault current	× No report about voltage compensation × No coordinated strategy for reactive power injection	[24]
	Presenting a cascaded controller to satisfy German GC requirements	✓ Soft switch of the MG from grid connected to isolated mode and vice versa	× Equal capacity of the DGs used for simulation	[26]
	Applying continuous mixed *p*-norm (CMPN) algorithm-based adaptive PI controller to the PV power plants	✓ Good dynamic response	× Lack of reactive current sharing strategy	[27]
The proposed algorithm	•Applying German GC reactive power support in the secondary layer •Implementing reverse droop per phase in power loop of the first layer, so that each phase of DGs can be controlled separately •Calculating the reference currents of the phases according to the reference powers of each phase •Using FOSMC for tracking the reference currents of positive- and negative-sequences in *dq* frame •Using a PI control for tracking the zero-sequence current	✓ Voltage compensation ✓ Reactive power sharing between the DGs ✓ Realizing GC requirements ✓ Reducing voltage imbalance factor originated from asymmetrical voltage sags ✓ Fast and accurate response of the FOSMC compared to the conventional PI ✓ Cost-effective ✓ Applicable to all of the inverter-based MGs	× Not considering the strength of the power grid during LVRT situation × Not considering the MGs including both Grid-Forming and the Grid-Following DGs	-

cases, and the power references are determined offline, which seems not applicable to real conditions [25]. A cascaded control loop for MG is presented in [26] to satisfy GCs in grid-connected mode, while the voltage magnitude has not been compensated in the inverter terminals. Additionally, the asymmetrical faults were not assessed in that research. Generally, the most significant issue with the current grid-following works like [27] is the lack of reactive current sharing strategy between the power sources during symmetrical and asymmetrical voltage disturbances, which should be addressed accurately. Table 1 provides a brief overview of this literature in which advantages and disadvantages of the reviewed papers are given. This table also gives information regarding the proposed method focusing on its novelties and practical implementation, either of which simplifies the objectives of this study. Finally, the mentioned drawbacks of this paper which are given in Table 1 can pave the way for further investigation in this literature.

1.3. Contribution and organization

Generally, the drawbacks of the reviewed studies can be summarized as follows. Firstly, most studies have considered grid-forming solutions, and grid-forming-based approaches cannot provide the exact amount of required reactive power during LVRT situations as is realized from [20]. Secondly, the lack of a coordinating strategy for reactive power-sharing is a striking weakness of the recent studies since the LVRT capability of the multi-source MGs has not been studied sufficiently [5,20,28,29]. Thirdly, operation capability under the asymmetrical voltage sags is important, which is not covered by some papers. Finally, the dynamic response of the inverters is a significant factor that can be improved by designing more accurate controllers like sliding mode control (SMC) [30], which was not considered in recent studies. Therefore, to address the mentioned gaps, a control scheme is proposed to improve the LVRT capability of the three-phase four-wire MGs based on independent control of each phase. For this purpose, reverse-droop control is used to regulate the voltage magnitude of each phase, followed by a fast response fractional-order SMC (FOSMC). Also, a secondary layer is designed to specify and share the reactive power references between the sources based on the free capacity of each DG phase. The existence of the second layer becomes crucial when the local reactive load is fed internally through the MG. It should be noted that in the previous studies, the local reactive load was considered zero or fed by the main grid. The main contributions of this paper are as follows:

- Proposing a two-layer control scheme for improving the LVRT capability of the MG in which each phase of the inverters is controlled separately. Therefore, the voltage of the safe phases will not be affected during the LVRT situation.
- Sharing the requested reactive power between the inverters in the faulty phases via the secondary layer of the presented controller. The voltage of the faulty phases can be compensated in point-of-common-coupling (PCC). This scheme can be used for all of the inverter-based systems.
- Implementing a nonlinear FOSMC and comparing it with the conventional PI and SMC methods in terms of accuracy and fast response, which proves outperformance of the FOSMC.
- Keeping the power quality indexes such as total harmonic distortion (THD) and voltage imbalance factor in acceptable range during LVRT conditions.
- Validating the proposed methodologies by real-time results.

The rest of the paper is organized as follows: The sequence analysis is performed in Section 2. Next, the proposed control layers are described in Section 3. Then, Section 4 is allocated to the introduction of the studied MG. Besides, this section shows the effectiveness of the simulations performed in MATLAB/Simulink and real-time set-up. Finally, in last section this work is concluded.

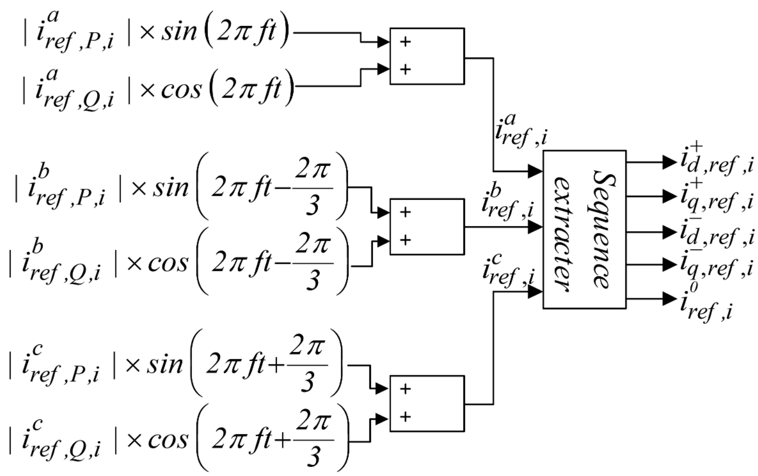

Fig. 2. Reference current generation of *i*th inverter and sequence extractor unit.

2. Sequence analysis during faulty conditions

In this section, necessity of decomposing the three-phase voltage and current into positive, negative, and zero sequence is discussed. Moreover, the results of extracting sequence values of the voltage and current in the *dq0* is shown via equations for three-wire and four-wire systems.

Every balanced or unbalanced three-phase system can be divided into three balanced systems as below:

$$X_{abc} = \begin{cases} X_a^+ + X_a^- + X_a^0 \\ X_b^+ + X_b^- + X_b^0 \\ X_c^+ + X_c^- + X_c^0 \end{cases} \tag{1}$$

Where, (+, −-, *0*) superscripts denote positive, negative, and zero-sequences of *X*, respectively. However, negative and zero-sequences only emerge during asymmetrical conditions. As stated earlier, asymmetrical faults are more likely to happen compared to symmetrical perturbations. Hence, in case of fault occurrence, sequence values should be extracted. In three-wire systems, the zero-sequence does not exist since there is no path for it to flow. Accordingly, only positive and negative sequences of current must be injected for voltage compensation in these systems. Furthermore, the current and voltage values are transformed into *dq* coordinates for comfortably controlling the injected active and reactive currents during the faults. Thus, the voltage and current can be written as:

$$\begin{aligned} v &= \vec{v}_d + \vec{v}_q = \overrightarrow{\left(v_d^+ + v_d^-\right)} + \overrightarrow{\left(v_q^+ + v_q^-\right)} \\ i &= \vec{i}_d + \vec{i}_q = \overrightarrow{\left(i_d^+ + i_d^-\right)} + \overrightarrow{\left(i_q^+ + i_q^-\right)} \end{aligned} \tag{2}$$

Unlike three-wire circuits, four-wire systems provide the path for zero-sequence. However, because the LVRT capability of these systems has not been studied sufficiently, the zero-sequence term is used less for voltage compensation. Thus, (2) can be modified as below for the systems with neutral wire:

$$\begin{aligned} v &= \vec{v}_d + \vec{v}_q + \vec{v}_0 = \overrightarrow{\left(v_d^+ + v_d^-\right)} + \overrightarrow{\left(v_q^+ + v_q^-\right)} + \vec{v_0^0} \\ i &= \vec{i}_d + \vec{i}_q + \vec{i}_0 = \overrightarrow{\left(i_d^+ + i_d^-\right)} + \overrightarrow{\left(i_q^+ + i_q^-\right)} + \vec{i_0^0} \end{aligned} \tag{3}$$

Where, v_0^0 and i_0^0 represent zero components of zero-sequence in *dq0* frame for voltage and current. It should be noted that, unlike positive and negative sequences, in this paper, the zero-sequence current is injected in *abc* coordinate rather than *dq0*.

3. Proposed reactive power control of MGs during LVRT condition

In this study, two control layers are designed to manage the reactive power of each phase separately. In the primary layer, the reverse-droop is embedded. Besides, FOSMC is designed for controlling the positive and negative sequences of the current in the *dq* frame. On the other hand, zero-sequence current is injected using PI controllers in abc frame. Also, the secondary layer compares the voltage of each phase with nominal values to detect if any sag has occurred. Then, in case of voltage sag incidences, this layer determines the required reactive power using GC and the proposed power-sharing scheme to satisfy the regulations. Finally, the required reactive power of DG phases is shared according to their free capacity. These amounts are sent to the primary layer through low-bandwidth communicational infrastructures. The following subsections describe the proposed layers with more details.

3.1. Primary layer

3.1.1. Reverse-droop control

In this layer, *Q–V* reverse droop functions regulate the voltage of each phase [31]. Also, the active power injection to each phase is controlled using *P–f* reverse droop, which can be applied as (4):

$$\begin{aligned} P_{rev,i}^{(j=abc)} &= \frac{1}{3}P_0^i + \frac{1}{m_{p,i}^j}\left(f_{rated} - f_i\right) \\ Q_{rev,i}^{(j=abc)} &= \frac{1}{3}Q_0^i + \frac{1}{n_{q,i}^j}\left(V_{rated} - V_i^j\right) \end{aligned} \tag{4}$$

In this paper, the *i* and *j* indices are respectively used to point to *i*th DG and phase *j*. So, $P_{rev,i}^j$ and $Q_{rev,i}^j$ refer to the active and reactive power output of reverse droop in DGs. Furthermore, P_0^i and Q_0^i are the constant three-phase active and reactive power injected by each DG. Also, f_{rated} and V_{rated} denote the rated values of frequency and voltage. The f_i and the V_i^j refer to the measured frequency and voltage of DGs. In addition, $1/m_{p,i}$ and $1/n_{q,i}$ are slopes of the *P–f* and *Q–V* functions.

3.1.2. Reference current generation

The process of reference current generation for each phase of the DGs is shown using (5) and Fig. 2:

$$\begin{aligned} \left|i_{ref,p,i}^j\right| &= \frac{2 \times P_{ref,i}^j}{\left|V_i^j\right|} \\ \left|i_{ref,Q,i}^j\right| &= \frac{2 \times Q_{ref,i}^j}{\left|V_i^j\right|} \end{aligned} \tag{5}$$

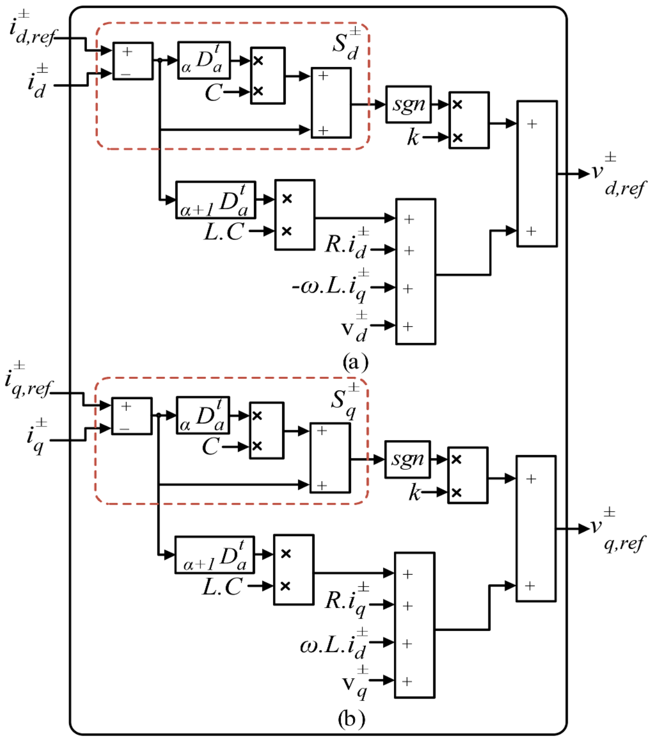

Fig. 3. FOSMC block diagram of a grid-following inverter in a) d^{+-}; b) q^{+-}.

Eq. (5) defines the magnitude of active and reactive reference currents based on reference powers of the corresponding phases. Thus, $P^j_{ref,i}$ and $Q^j_{ref,i}$ represent active and reactive power references, and $|V^j_i|$ shows the voltage magnitude. The active power reference is considered equal to active power output of the reverse droop, and the reactive power reference value is discussed in the following. The calculation of reference currents of DG phases beside positive and negative sequence extraction in *dq* frame ($i^{\pm}_{dq,ref,i}$) is also shown in Fig. 2. According to this figure, active and reactive current references of the phases are added together to form a three-phase sinusoidal waveform for reference currents. Then, the references in abc frame are transformed into the dq frame. Finally, positive and negative sequences of the reference currents are extracted in the *dq* coordinate, which are inputs of the FOSMC controller. In addition, the zero-sequence reference current ($i^0_{ref,i}$), which only exists in four-wire systems, is extracted in the natural frame, and it is the input of the zero-sequence control unit.

3.1.3. FOSMC design

In this paper, FOSMC is used for controlling current, since SMC-based controllers are robust to parameter uncertainties and can mitigate dynamic instabilities resulting from grid faults [32,33]. The main difference between the FOSMC and conventional SMC approaches is order of the sliding surface that can be shown using ${}_aD^t_\alpha$ operator [34]. The α (alpha) in the operator refers to the order of the sliding surface that can be non-integer in case of FOSMC. Also, a and t denote the operation boundaries. This operator is defined as below:

$$ {}_aD^t_\alpha = \begin{cases} \dfrac{d^\alpha}{dt^\alpha} & \alpha > 0 \\ 1 & \alpha = 0 \\ \displaystyle\int_a^t (d\tau)^\alpha & \alpha < 0 \end{cases} \tag{6} $$

In this paper, (7) and (8) are utilized to estimate the fractional-order differo/integral transfer function:

$$ \begin{aligned} &\mathrm{G(s)} = \mathrm{S}^\alpha,\ \alpha \in \mathrm{R} \\ &\hat{\mathrm{G}}(\mathrm{s}) = \mathrm{H}\prod_{\mathrm{k}=-\mathrm{N}}^{\mathrm{N}} \frac{\mathrm{s}+\omega_\mathrm{k}'}{\mathrm{s}+\omega_\mathrm{k}} \end{aligned} \tag{7} $$

Where, N refers to estimation order. Also, ω_k' and ω_k denote zeros and poles of the estimated transfer function shown in (8). Moreover, the terms ω_b and ω_h in (8) are respectively lower and higher frequencies.

$$ \begin{aligned} &\omega_\mathrm{k}' = \omega_\mathrm{b}\cdot\left(\frac{\omega_\mathrm{h}}{\omega_\mathrm{b}}\right)^{(\mathrm{k+N+0.5(1-\alpha)})(2\mathrm{N}+1)} \\ &\omega_\mathrm{k} = \omega_\mathrm{b}\cdot\left(\frac{\omega_\mathrm{h}}{\omega_\mathrm{b}}\right)^{(\mathrm{k+N+0.5(1+\alpha)})(2\mathrm{N}+1)} \\ &\qquad \mathrm{H} = \omega_\mathrm{h}^\alpha \end{aligned} \tag{8} $$

Having defined the primary descriptions, state-space equations of the three-phase inverters are also required to model the DC/AC inverter, which is explained in *dq* frame as below:

$$ \begin{aligned} \frac{di_d^\pm}{dt} &= -\frac{R}{L}i_d^\pm + \omega i_q^\pm + \frac{Sw_d^\pm}{L}V_{DC} - \frac{1}{L}\mathrm{V}_d^\pm + \Delta_d^\pm \\ \frac{di_q^\pm}{dt} &= -\frac{R}{L}i_q^\pm - \omega i_d^\pm + \frac{Sw_q^\pm}{L}V_{DC} - \frac{1}{L}\mathrm{V}_q^\pm + \Delta_q^\pm \end{aligned} \tag{9} $$

Where, R, L, V_{DC}, $Sw^{\pm}_{dq}$, and $\Delta^{\pm}_{dq}$ respectively represent the resistance and inductance of the inverter filter, constant DC voltage, switching states of the inverters that can adopt 0 or 1, and filter uncertainties. Moreover, $V^{\pm}_{dq}$ and $i^{\pm}_{dq}$ respectively show measured values of terminal voltage and output current of the inverters using positive and negative sequences in the *dq* frame. Then, fractional sliding surfaces and input control signals are respectively determined like (10) and (11):

$$ \begin{aligned} S_d^\pm &= \left(i_{d,ref}^\pm - i_d^\pm\right) + C\cdot{}_aD^t_a\left(i_{d,ref}^\pm - i_d^\pm\right) \\ S_q^\pm &= \left(i_{q,ref}^\pm - i_d^\pm\right) + C\cdot{}_aD^t_a\left(i_{q,ref}^\pm - i_q^\pm\right) \end{aligned} \tag{10} $$

$$ \begin{aligned} v_d^\pm &= Sw_d^\pm . V_{DC} \\ v_q^\pm &= Sw_q^\pm . V_{DC} \end{aligned} \tag{11} $$

In (10), $i^{\pm}_{dq,ref}$ shows the reference currents of the sequences in the *dq* frame. Besides, C is the gain of the mentioned operator. Next, the control law that comprises of equivalent input and switching function is derived by meeting $S = 0$ and $\dot{S} = 0$. Therefore, Eq. (12) can be described as:

$$ \begin{aligned} v_{d,eq}^\pm &= Ri_d^\pm - \omega Li_q^\pm + V_d^\pm + LC\cdot{}_{\alpha+1}D^t_a\left(i_{d,ref}^\pm - i_d^\pm\right) \\ v_{q,eq}^\pm &= Ri_q^\pm + \omega Li_d^\pm + V_q^\pm + LC\cdot{}_{\alpha+1}D^t_a\left(i_{q,ref}^\pm - i_q^\pm\right) \end{aligned} \tag{12} $$

Also, the switching function is written as:

$$ v_s^{dq\pm} = k.\mathrm{sgn}\left(S_{dq}^\pm\right) \tag{13} $$

In (13), k shows the switching gain. Overall, $v^{\pm}_{d,ref}$ and $v^{\pm}_{q,ref}$ can be defined as:

$$ \begin{aligned} v_{d,ref}^\pm &= Ri_d^\pm - \omega Li_q^\pm + V_d^\pm + L.C.{}_{\alpha+1}D^t_a\left(i_{d,ref}^\pm - i_d^\pm\right) + k.\mathrm{sgn}\left(S_d^\pm\right) \\ v_{q,ref}^\pm &= Ri_q^\pm + \omega Li_d^\pm + V_q^\pm + L.C.{}_{\alpha+1}D^t_a\left(i_{q,ref}^\pm - i_q^\pm\right) + k.\mathrm{sgn}\left(S_q^\pm\right) \end{aligned} \tag{14} $$

The overall block diagram of the FOSMC is depicted in Fig. 3. Also, the Lyapunov function is usually used to evaluate the sliding mode controllers in terms of stability. This equation is permanently positive, and its derivative must be a negative amount to draw the system into a stable margin. Eq. (15) represents the Lyapunov function and the condition that needs to be met:

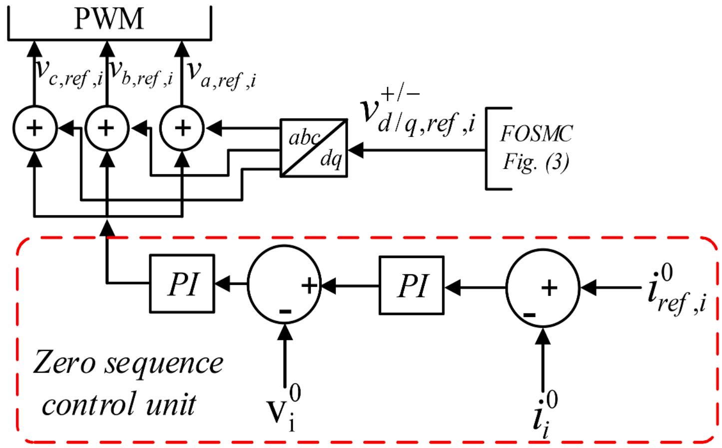

Fig. 4. Block diagram of the zero-sequence control unit.

$$V = \frac{1}{2} S_{dq}^{\pm\,T} S_{dq}^{\pm}$$
$$\frac{dV}{dt} = S_{dq}^{\pm\,T} \cdot \frac{dS_{dq}^{\pm}}{dt} < 0 \tag{15}$$

Thus, (16) has to be met to keep the system in stable margin:

$$S_{dq}^{\pm}\left(\frac{-k}{L}\operatorname{sgn}\left(S_{dq}^{\pm}\right) - \Delta_{dq}^{\pm}\right) < 0$$
$$k_{dq}^{\pm} < L\Delta_{dq}^{\pm} \tag{16}$$

3.1.4. Zero-sequence control unit

This control unit contains two PI controllers for generating reference voltages of zero-sequence. Fig. 4 highlights this control unit and the way inverters injects the zero-sequence current into the grid.

In Fig. 4, i_i^0 and V_i^0 are respectively the measured zero-sequence current and voltage of the *i*th inverter.

3.2. Secondary layer

Reactive power injection is an important function during the LVRT situation. Thus, the proposed secondary layer tries to support the grid by determining the reactive power share of each phase of the DGs. The total amount of requested reactive power by GC for each phase is inferred from Fig. 1b, and follows (17) while there is a local reactive load inside the MG:

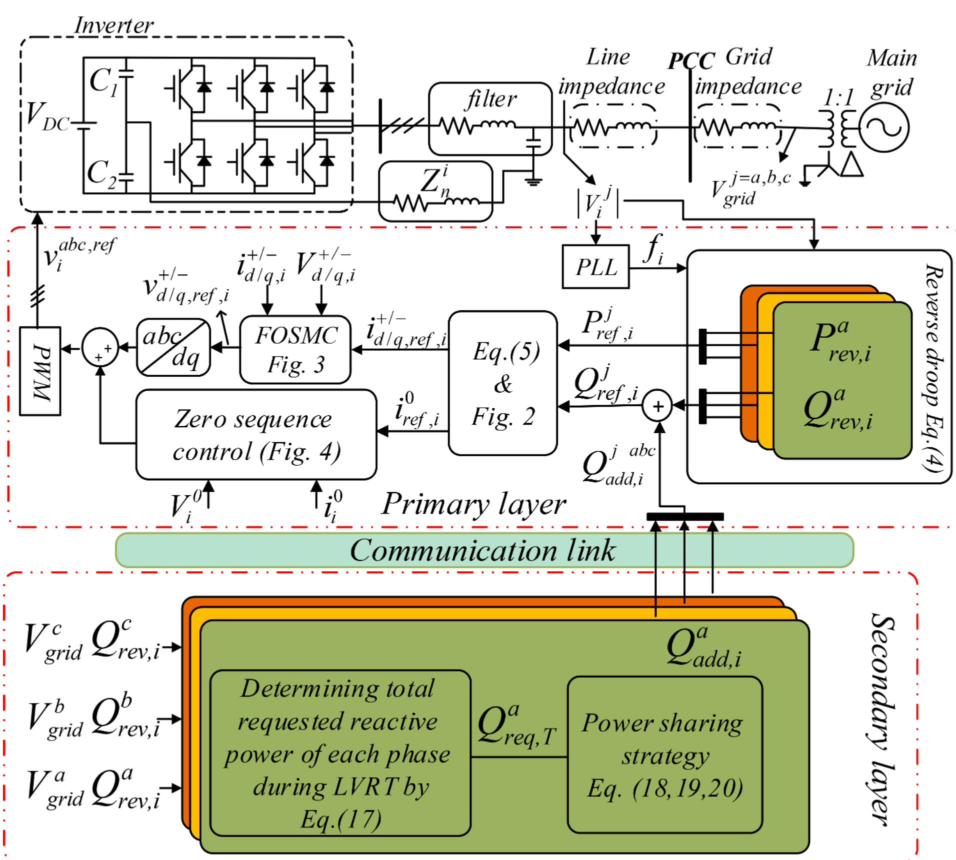

Fig. 5. The proposed coordinated reactive power control of the MG with independent phase control of *i*th inverters.

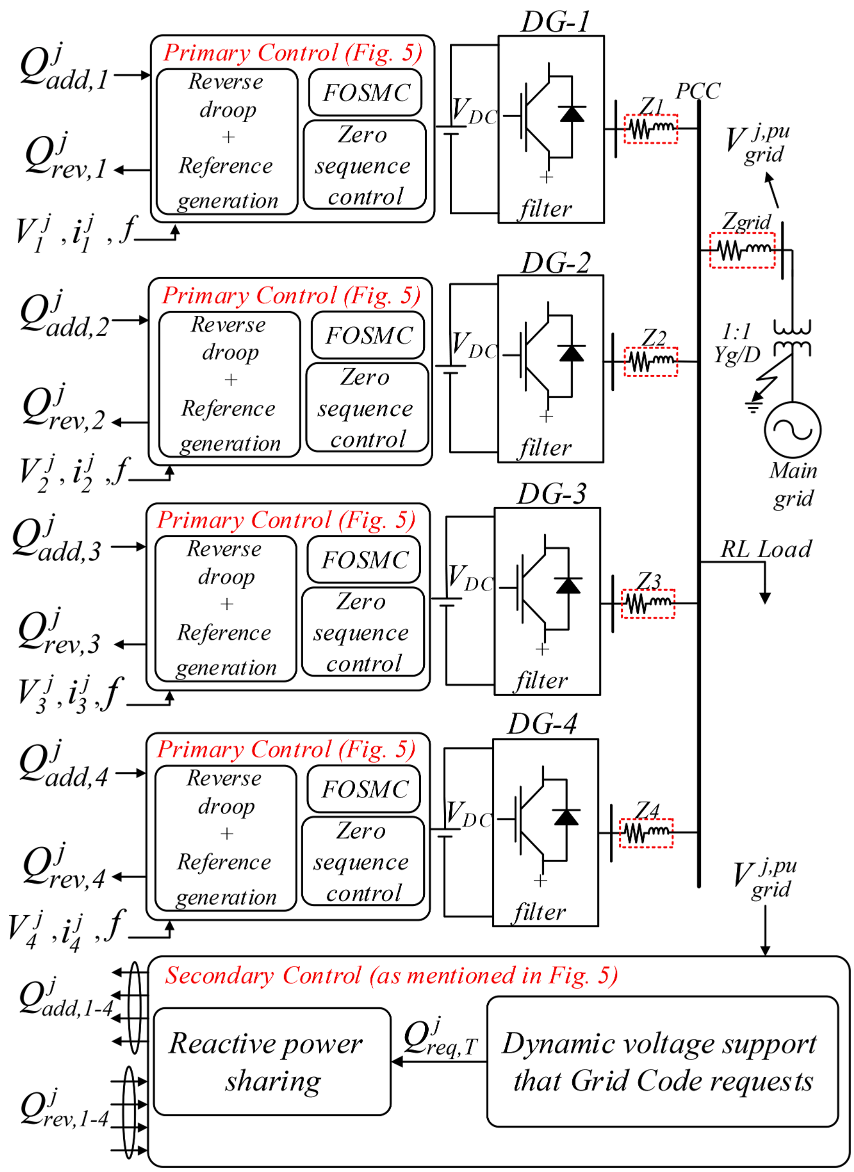

Fig. 6. The studied grid-tied grid-following MG structure.

$$Q^j_{req,T} = \begin{cases} 0 & V^{j,pu}_{grid} \geq 0.9 \\ -\frac{1}{3}S_{rated,MG} & V^{j,pu}_{grid} \leq \frac{1}{2}\left(1 + \frac{\frac{1}{3}Q^0_i}{\frac{1}{3}S_{rated,MG}}\right) \\ \left(-K \times \left(1 - V^{j,pu}_{grid}\right) \times \frac{1}{3}S_{rated,MG}\right) - \frac{1}{3}Q^0_i & otherwise \end{cases} \tag{17}$$

In (17), $V^{j,pu}_{grid}$ and $S_{rated,MG}$ respectively represent the standardized voltage magnitude of the main grid and rated capacity of the MG. Furthermore, K is the rate of voltage compensation, which is considered 2 as German GC. Next, the additional reactive power of each phase of the DGs ($Q^j_{add,i}$) are calculated according to (18)–(20):

$$Q^j_{add,T} = -Q^j_{req,T} - \sum_i Q^j_{rev,i} \tag{18}$$

$$S^j_{empty,i} = \frac{1}{3}S_{rated,i} - Q^j_{rev,i} \tag{19}$$

$$Q^j_{add,i} = \frac{S^j_{empty,i}}{\sum_i S^j_{empty,i}} \times Q^j_{add,T} \tag{20}$$

The terms $Q^j_{add,T}$ and $S^j_{empty,i}$ refer to the total additional reactive power and the empty capacity of phase j. Generally, the reactive power reference for each phase can be obtained as:

$$Q^j_{ref,i} = Q^j_{rev,i} + Q^j_{add,i} \tag{21}$$

In addition, a communicational infrastructure is required to convey the reactive power amounts from the first layer to the second layer and vice versa, with T_d delay. It can be defined as:

$$G(s) = \frac{1}{1 + T_d s} \tag{22}$$

The overall block diagram of the proposed two-layer controller is pointed out in Fig. 5.

Table 2
Parameters of the system and the proposed controller.

Test system and control parameters	
Filters of DG_1 (R, L, C), Z_1	0.1 Ω, 3 mH, 40 μF), 0.3 mH
Filters of DG_2 (R, L, C), Z_2	(0.1 Ω, 3.5 mH, 40 μF), 0.3 mH
Filters of DG_3 (R, L, C), Z_3	(0.1Ω, 3mH, 40μF), 0.3mH
Filters of DG_4 (R, L, C), Z_4	(0.1Ω , 4 mH, 40 μF), 0.3 mH
C_1, C_2 (Fourth leg)	1000 μF, 1000 μF
Z_{grid}, $Z_n^{i=1-4}$(fourth wire)	1.4 mH, 0.1 Ω + 0.6 mH
V_{DC}, V_{AC}, frequency	800 v, 380 v, 50 Hz
Rated kVA (S_{rated}) of DG_{1-4}	53, 40, 53, 35
Local load	75 kW + 15 kVAR
$m_{p,1}^j$, $m_{p,2}^j$, $m_{p,3}^j$, $m_{p,4}^j$	0.0003, 0.0004, 0.0003, 0.0005
$n_{q,1}^j$, $n_{q,2}^j$, $n_{q,3}^j$, $n_{q,4}^j$	0.0013, 0.0017, 0.0013, 0.0020
$k_{dq}^{\pm}$, $C_{dq}^{\pm}$	1, 50,000
Switching frequency	10 kHz
K (Voltage compensation rate)	2 pu
N	5
ω_b	0.0001 Hz
ω_h	10,000 Hz

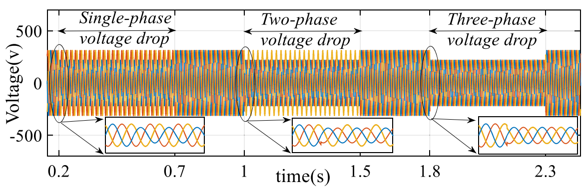

Fig. 7. Implemented symmetrical and asymmetrical voltage sags to main grid.

4. Simulation and real-time results

4.1. Micro-grid configuration

The case study system is a grid-connected MG composed of four parallel inverter-based DGs. The capacity of the sources is 53 kVA, 40 kVA, 53 kVA, and 35 kVA. Additionally, the DGs are operating in 70 % of their rated capacity in normal condition. Also, an RL load (75 kW +15 kVA) exists in the MG, which is fed locally by the DG1. The studied MG is shown in Fig. 6, and the system's parameters of the MG and the proposed controller are provided in Table 2.

4.2. Simulation results

Several scenarios including symmetrical and asymmetrical voltage sags are implemented to the main grid to assess the performance of the proposed controller in compensating PCC voltage and fulfilling GC requirements. The implemented disturbances are 30 % single-phase, two-phase, and three-phase voltage sags that happen at t =0.2 s, 1 s, and 1.8 s. All of the perturbations last for 0.5 s, which are shown in Fig. 7.

After voltage drop, the sources of the MG start injecting reactive power into the faulty phases according to the GC and the proposed method in the second layer. The reactive power output of the DG phases is depicted in Fig. 8, which proves that the operation of the MG complies with German GC in terms of reactive power injection. Also, Table 3 shows the reactive power reference of the DG phases determined by German GC and compares them with the injected amounts extracted from Fig. 8. Furthermore, the exchanged reactive power between the main grid and the MG alongside the reference values is shown in Fig. 9, which demonstrates that the reactive power exchange is done with slight error.

Reactive power injection raises the voltage of PCC and DGs by about 30 % in the faulty phases, as shown in Fig. 10, and it points out the exchanged current between the MG and the main grid. Besides, the magnitude of PCC voltage for each phase is shown in Fig. 11. Moreover, the local load is appropriately fed during normal and LVRT conditions,

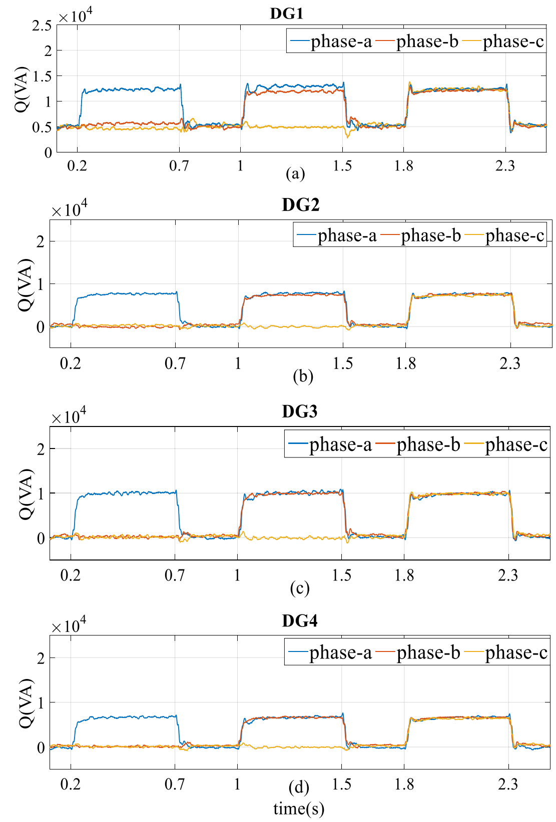

Fig. 8. Injected reactive power of a) DG_1; b) DG_2; c) DG_3; d) DG_4.

highlighted in Fig. 12. In addition, the terminal voltage of the sources is compensated by30 % and restored to the pre-fault condition, which verifies that the LVRT requirement of the GC is fulfilled by injecting reactive power to the disturbed phases. The compensated terminal voltage of DG-1 is depicted in Fig. 13, besides its output current in three different cases. However, because of space lack, voltage, and current waveforms of the other DGs are not highlighted in the paper. Overall, the analysing of the results, concludes that compliance with the GC, which is one of the main goals of the proposed controller, is achieved.

On the other hand, the presented control strategy guarantees that voltage imbalance factors of different MG spots remain in the acceptable range during symmetrical and asymmetrical voltage conditions. This claim is shown in Table 4 and calculated by dividing the magnitude of negative sequence voltage by the positive sequence. The voltage imbalances have not risen above 2 %, which is the recommended percentage by IEEE 1159 for normal operations [35]. Moreover, voltage and current THD percentages are reported in Table 5 during the mentioned case studies.

4.3. Comparison of FOSMC with conventional SMC and PI methods

Simulations are repeated to find the best value of alpha in integral mode, for which the dynamic response, accuracy, and speed are the highest. On the other hand, by setting the alpha to an integer value such as one, the controller can be changed to conventional SMC. In addition, the control scheme is also designed via tuned PI controllers for comparison purposes. Therefore, the exchanged reactive power of each phase in PCC is evaluated during single-phase and two-phase 30 % voltage sags, which are depicted through Figs. 14 and 15, respectively. Assessing Figs. 14 and 15 declares that the performance of the proposed reactive power control strategy is the best when alpha is set to 0.76. The conventional tuned PI control is inaccurate as shown in Figs. 14 and 15. In addition, the conventional SMC method performs far better than PI in

Table 3
Comparing the injected reactive power of each DG phase with the reference values of the German GC during 30 % sag.

	Injected reactive power of each phase of the DGs by proposed method (kVA)			Reference reactive power of the DG phases in German GC (kVA)		
	Phase-a	Phase-b	Phase-c	Phase-a	Phase-b	Phase-c
DG_1	12.5	12.7	12.5	12.6	12.6	12.6
DG_2	7.85	7.8	7.85	8	8	8
DG_3	10.2	10.2	10.2	10.6	10.6	10.6
DG_4	6.75	6.7	6.7	7	7	7

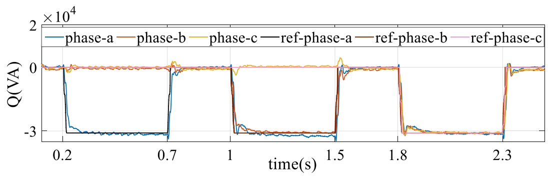

Fig. 9. Exchanged reactive power between MG and main grid in PCC.

terms of accuracy and dynamic response. However, evaluating Fig. 15a points out that the SMC suffers from error while tracking the reference amount of reactive power. Nevertheless, by setting the alpha to 0.76, the tracking accuracy and speed improves and becomes better than other fractional orders and the SMC approach. It can be concluded that, flexibility of the FOSMC approach in selecting control order can improve the response of control system.

In addition, the FOSMC and PI control methods are compared in terms of Mean-Percentage-Absolute-Error (MPAE) index during asymmetrical voltage sags. As demonstrated in Table 6, the MPAE value of the

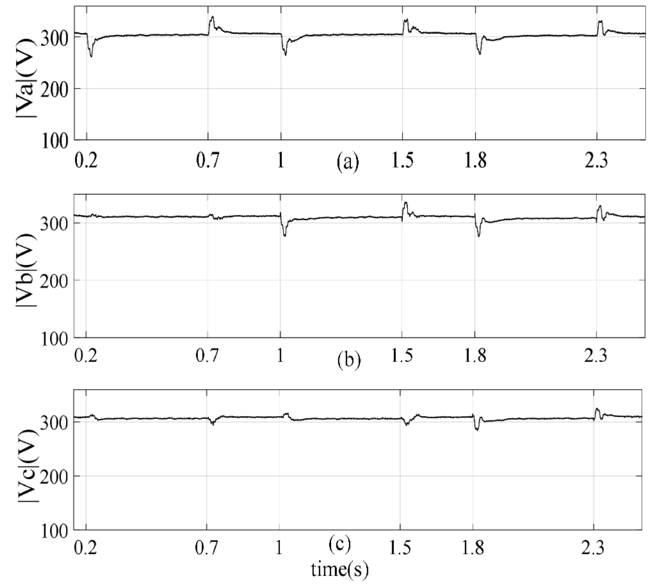

Fig. 11. PCC voltage magnitude during symmetrical and asymmetrical voltage drops in a) phase-a, b) phase-b, c) phase-c.

phase-a and phase-b are calculated via (23) in a condition when a filter uncertainty exists. In (23), n refers to the number of the samples, while y_i and y_i^{ref} represent the parameter and its reference value, for which MPAE is intended to be calculated. According to Table 6, outperformance of the FOSMC controller is obvious as it has lower amounts of errors compared to the conventional PI control for different values of

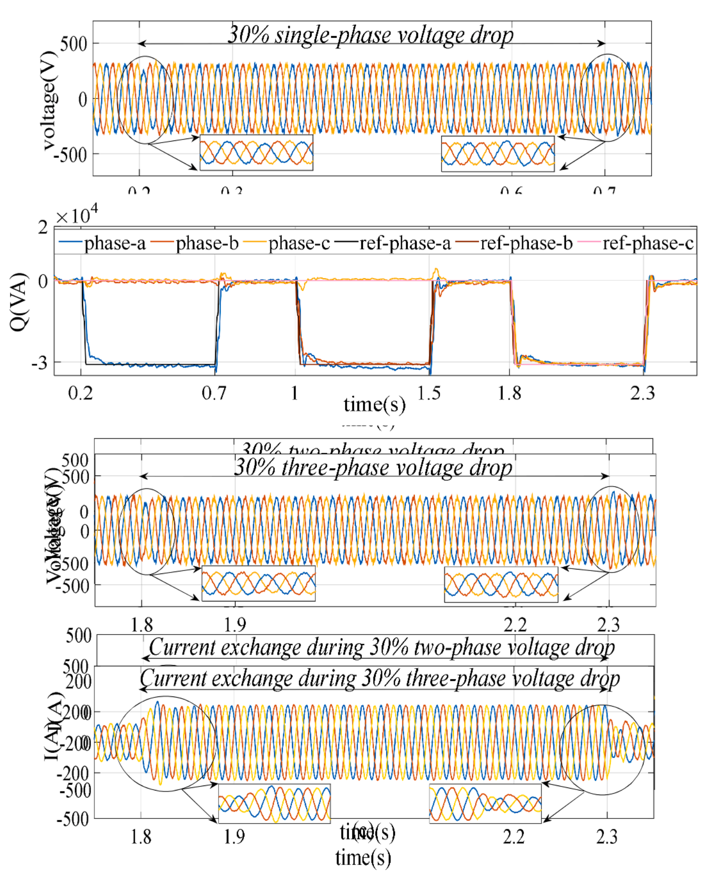

Fig. 10. Compensated voltage and exchanged current of PCC during a) single-phase; b) two-phase; c) three-phase voltage drops.

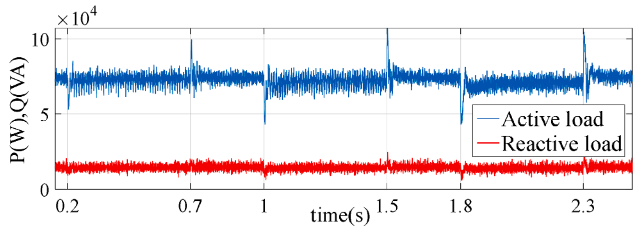

Fig. 12. Active and reactive load of the MG.

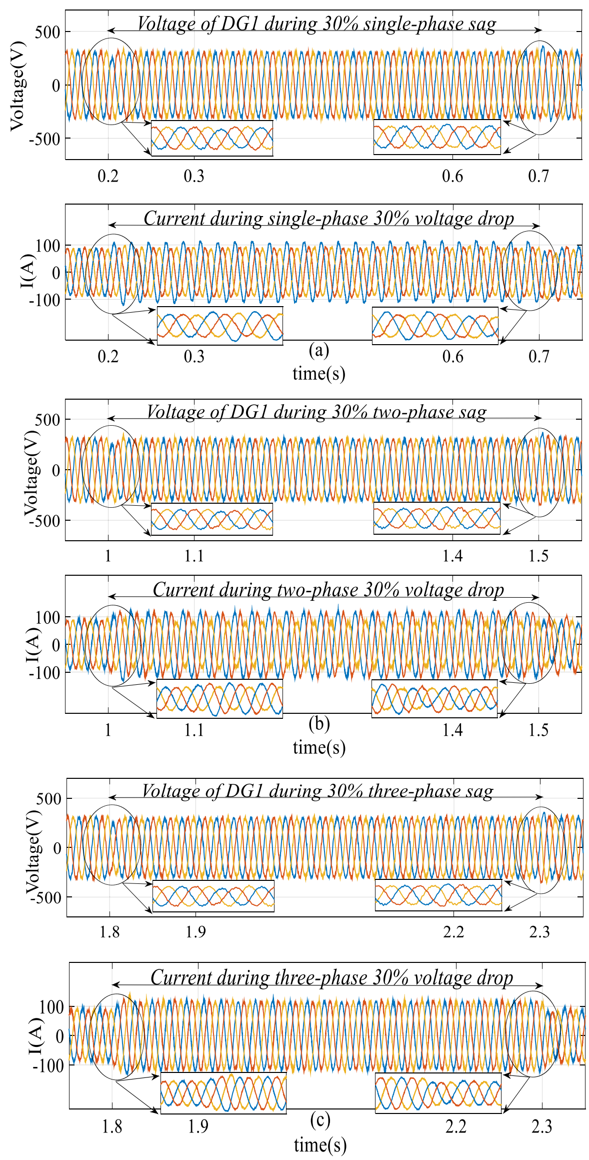

Fig. 13. Restored Voltage and output current waveforms of DG_1 during 30 % a) single-phase; b) two-phase; c)three-phase voltage sags.

inductance filter. So, it can be concluded that the FOSMC is a more robust controller when it is compared to the PI controller in a similar condition.

$$MPAE(\%) = 100 \times \frac{1}{n}\sum_{i=1}^{n}\frac{y_i - y_i^{ref}}{y_i} \tag{23}$$

The FOSMC and PI controllers are also compared in terms of voltage compensation and THD values (voltage and current THD of the PCC) during single-phase (0.2–0.7 s), two-phase (1–1.5 s), and three-phase (1.8–2.3 s) voltage sag occurrences. As it is demonstrated in Fig. 16, the proposed FOSMC shows better performance against the conventional PI controller since it has better dynamic response at the initial moments of sags. On the other hand, power quality of the MG can be further improved via FOSMC during voltage sags as it is demonstrated in Table 7.

Table 4
Imbalance factor of voltage during different types of voltage sags.

	Voltage imbalance factor during 30 % voltage sags (%)		
	Single-phase	Two-phase	Three-phase
Grid	8.890	10	0
PCC	1.379	1.852	0.326
Load	1.379	1.852	0.326
DG_1	1.370	1.838	0.329
DG_2	1.376	1.840	0.330
DG_3	1.447	1.931	0.349
DG_4	1.444	1.932	0.346

Table 5
Voltage and current THD during voltage sags.

	Voltage and current THD (%) during 30 % voltage sags					
	Single-phase		Two-phase		Three-phase	
	THD_v	THD_i	THD_v	THD_i	THD_v	THD_i
PCC	3.74	3.05	4.89	3.12	4.03	2.49
Load	3.74	2.67	4.89	3.23	4.03	2.53
DG_1	4.03	4.93	5.19	5.05	4.23	3.82
DG_2	3.94	3.99	5.01	3.87	4.31	4.43
DG_3	3.96	4.10	5.12	4.17	4.22	3.76
DG_4	3.97	4.78	5.13	5.58	4.27	4.60

4.4. Real-time results

The real-time analysis is carried out through the setup highlighted in Fig. 17. For this purpose, the host computer is used to model the inverters and controller of the studied MG. Then, the code is downloaded to the target PC [31]. The system model runs on the target PC and is solved by ode 4 (Rung–Kutta) with a sample time of 0.01 ms. Also, the target and host PCs are linked together using an RS232 serial card. The real-time results which validate the simulations are depicted in Figs. 18 and 19.

5. Conclusion

MGs integration into power systems has boosted the system's reliability and caused operational challenges for the network operators. Hence, some countries have considered a set of requirements to improve the functionality of their power systems. For this purpose, in this paper, an LVRT scheme is proposed for four-wire MGs, which can control each phase of the DGs independently through a grid-following method. The local controller of the DGs, known as the primary layer, utilizes reverse-droop control for voltage and frequency regulation and a nonlinear FOSMC. On the other hand, the secondary layer fulfills the modern GC requirements by calculating the required reactive power for the faulty phases. Next, this amount is shared between the corresponding phases of the DGs based on their free capacity. The effectiveness of the presented controller is proved by analyzing the results obtained from implementing 30 % single-phase, two-phase, and three-phase voltage sags. Accordingly, each DG phase injects reactive power during voltage sags according to the determined amount. Also, comparing the injected reactive power with the amounts of German GC demonstrates that the reactive power injection is done with acceptable accuracy. The results point out that during the external sags, the voltage of PCC, inverter terminals, and load terminals are restored to their nominal values, 30 % compensation, as if there is no perturbation. Consequently, the

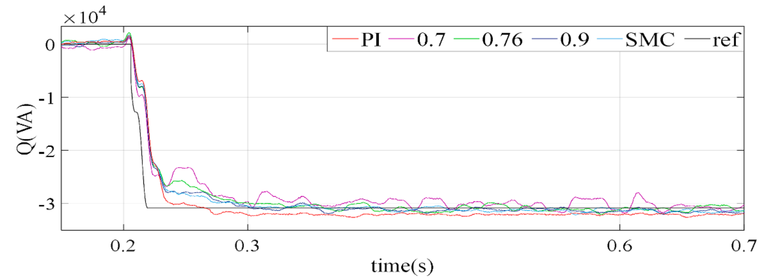

Fig. 14. Exchanged reactive power between the MG and main grid in phase-a during single-phase voltage drop using conventional methods and different fractional values for alpha.

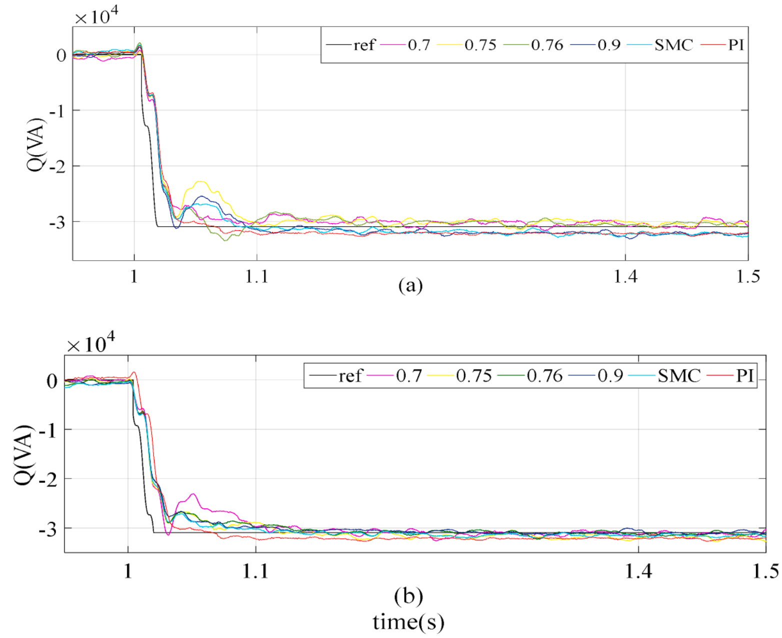

Fig. 15. Exchanged reactive power between the MG and main grid in a) phase-a; b) phase-b during two-phase voltage drop using conventional methods and different fractional values for parameter alpha.

Table 6
MPAE value of the exchanged reactive power of the MG and main grid during asymmetrical voltage sags using the FOSMC and PI control (%).

Voltage sag Type / Filter deviation	single-phase voltage sag		two-phase voltage sag			
	phase-a		phase-a		phase-b	
	MPAE Value (%)					
	FOSMC	PI	FOSMC	PI	FOSMC	PI
+40% (1.4L)	2.24	4.97	2.62	8.04	2.33	5.46
+20% (1.2L)	1.66	4.51	2.48	7.88	2.14	5.14
0% (L)	1.93	4.45	2.26	5	1.59	4.11
-20% (0.8L)	1.93	4.79	2.46	5	1.69	4.23
-40% (0.6L)	2.06	4.58	2.64	6.9	3.39	4.4

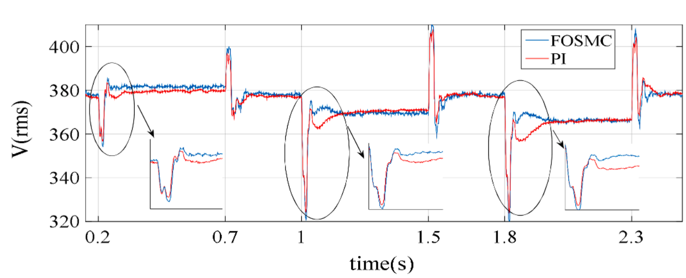

Fig. 16. RMS voltage of the PCC during 30 % symmetrical and asymmetrical voltage sags.

Table 7
THD values of PCC voltage and current during 30 % voltage sags.

	Voltage and current THD (%) during 30 % voltage sags in PCC					
	Single-phase		Two-phase		Three-phase	
	THD_v	THD_i	THD_v	THD_i	THD_v	THD_i
FOSMC	3.74	3.05	4.89	3.12	4.03	2.49
PI	5.28	3.28	5.29	3.45	5.71	2.99

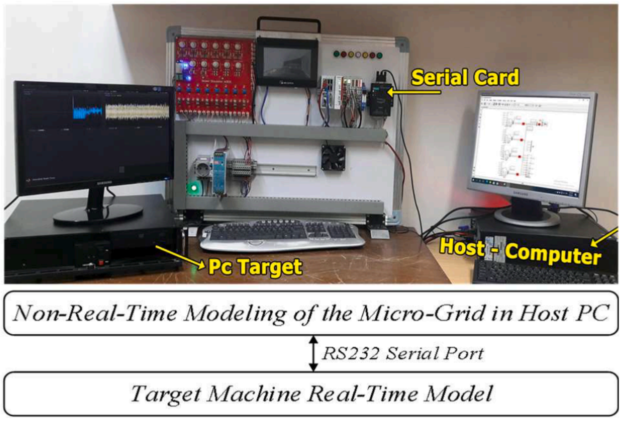

Fig. 17. Setup for implementing real-time simulations.

presented controller can realize the GC requirements and ride through during severe voltage conditions. Moreover, this control method keeps the power quality indices like THD and voltage imbalance factors in acceptable ranges during the sags. Also, the superiority of designed FOSMC over conventional current controllers such as PI and SMC are demonstrated. This outperformance is highlighted with several aspects such as MPAE index, THD values, voltage compensation, and reactive power tracking during the imposed voltage sags. It is shown that the best value for the alpha is 0.76, by which the response of the controller is fast and accurate. Finally, the simulations are validated through real-time results. Our future work is focused on the LVRT capability of the MGs including both grid-forming and grid-following inverters. In addition, the effect of grid strength and R/X ratio of the power lines can be discussed in the future investigations, which has not been addressed sufficiently in this literature.

CRediT author statement

Reza Deihimi Kordkandi: Methodology,
Mehrdad Tarafdar Hagh: Simulation,
Sam Roozbehani: Writing,
Mojtaba Feyzi: Supervision
Navid Bayati: Editing
Thomas Ebel: Editing

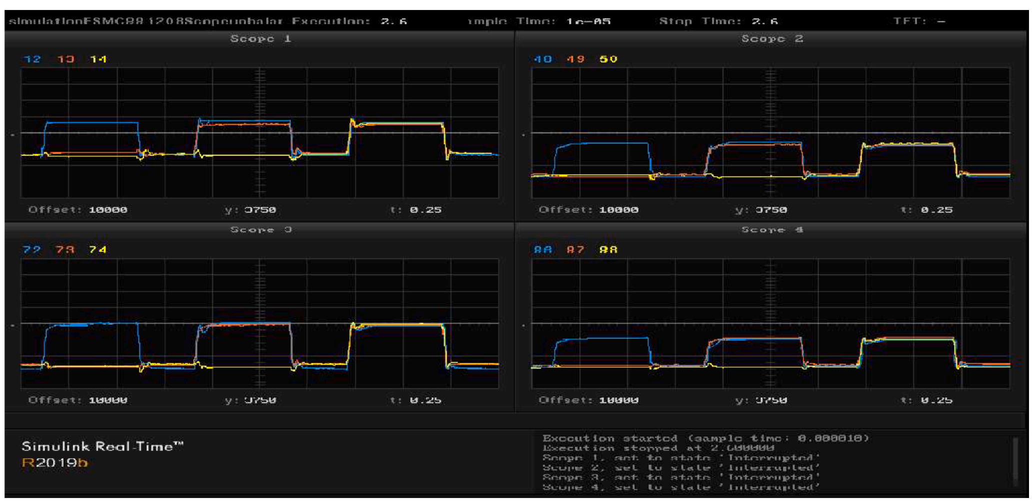

Fig. 18. Real-time results. Injected reactive power through each phase of a) DG1; b) DG2; c) DG3; d) DG4.

Fig. 19. Real-time results. a) Local active and reactive load. b) Waveform of the PCC voltage during symmetrical and asymmetrical voltage sags. c) Waveform of the PCC current injected to the main-grid during symmetrical and asymmetrical voltage sags. d) Exchanged active power between the MG and main grid during symmetrical and asymmetrical voltage drops.

Declaration of competing interest

The authors certify that they have NO affiliations with or involvement in any organization or entity with any financial interest (such as honoraria; educational grants; participation in speakers' bureaus; membership, employment, consultancies, stock ownership, or other equity interest; and expert testimony or patent-licensing arrangements), or non-financial interest (such as personal or professional relationships, affiliations, knowledge or beliefs) in the subject matter or materials discussed in this manuscript.

Data availability

No data was used for the research described in the article.

References

[1] K.A. Alobeidli, M.H. Syed, M.S. El Moursi, H.H. Zeineldin, Novel coordinated voltage control for hybrid micro-grid with islanding capability, IEEE Trans. Smart Grid 6 (3) (2015) 1116–1127.
[2] P. Piya, M. Ebrahimi, M. Karimi-Ghartemani, S.A. Khajehoddin, Fault ride-through capability of voltage-controlled inverters, IEEE Trans. Ind. Electron. 65 (10) (2018) 7933–7943.
[3] G.J. Kish, P.W. Lehn, Microgrid design considerations for next generation grid codes, in:, in: 2012 IEEE Power and Energy Society General Meeting, 2012, pp. 1–8.
[4] S. Ghosh, Y.J. Isbeih, R. Bhattarai, M.S. El Moursi, E.F. El-Saadany, S. Kamalasadan, A dynamic coordination control architecture for reactive power capability enhancement of the DFIG-Based wind power generation, IEEE Trans. Power Syst. 35 (4) (2020) 3051–3064.
[5] R.D. Kordkandi, M.T. Hagh, S. Roozbehani, Real-time low/high-voltage ride-through capability improvement of micro-grid based on coordinated robust grid-following control, IET Gener. Transm. Distrib. 16 (16) (2022) 3318–3332.
[6] Y.G. Painthankar, S.R. Bhide. *Fundermentals of Power System Protection*, 2022.
[7] I. Ngamroo, T. Karaipoom, Improving low-voltage ride-through performance and alleviating power fluctuation of DFIG wind turbine in DC microgrid by optimal SMES with fault current limiting function, IEEE Trans. Appl. Supercond. 24 (5) (2014) 1–5.
[8] F.-J. Lin, J.-C. Liao, C.-I. Chen, P.-R. Chen, Y.-M. Zhang, Voltage restoration control for microgrid with recurrent wavelet petri fuzzy neural network, IEEE Access 10 (2022) 12510–12529.
[9] A.V. Jayawardena. Contributions to the Development of Microgrids: Aggregated modelling and Operational Aspects, University of Wollongong, Wollongong NSW, Australia, 2015.
[10] L. Chen, et al., Comparison of superconducting fault current limiter and dynamic voltage restorer for LVRT improvement of high penetration microgrid, IEEE Trans. Appl. Supercond. 27 (4) (2017) 1–7.
[11] H. He, et al., Application of a SFCL for fault ride-through capability enhancement of DG in a microgrid system and relay protection coordination, IEEE Trans. Appl. Supercond. 26 (7) (2016) 1–8.
[12] A. Benali, M. Khiat, T. Allaoui, M. Denaï, Power quality improvement and low voltage ride through capability in hybrid wind-PV farms grid-connected using dynamic voltage restorer, IEEE Access 6 (2018) 68634–68648.
[13] F. Nejabatkhah, Y.W. Li, Overview of power management strategies of hybrid AC/DC microgrid, IEEE Trans. Power Electron. 30 (12) (2015) 7072–7089.
[14] B.M. Eid, N.A. Rahim, J. Selvaraj, A.H. El Khateb, Control methods and objectives for electronically coupled distributed energy resources in microgrids: a review, IEEE Syst. J. 10 (2) (2016) 446–458.
[15] A.G. Paspatis, G.C. Konstantopoulos, J.M. Guerrero, Enhanced current-limiting droop controller for grid-connected inverters to guarantee stability and maximize power injection under grid faults, IEEE Trans. Control Syst. Technol. 29 (2) (2021) 841–849.
[16] X. Zhao, J.M. Guerrero, M. Savaghebi, J.C. Vasquez, X. Wu, K. Sun, Low-voltage ride-through operation of power converters in grid-interactive microgrids by using negative-sequence droop control, IEEE Trans. Power Electron. 32 (4) (2017) 3128–3142.
[17] C. Li, X. Liu, K. Sun, Y. Cao, F. Ma, B. Zhou, A hybrid control strategy to support voltage in industrial active distribution networks, IEEE Trans. Power Deliv. 33 (6) (2018) 2590–2602.
[18] H.R. Baghaee, M. Mirsalim, G.B. Gharehpetian, Real-time verification of new controller to improve small/large-signal stability and fault ride-through capability of multi-DER microgrids, IET Gener. Transm. Distrib. 10 (12) (2016) 3068–3084.
[19] H.R. Baghaee, M. Mirsalim, G.B. Gharehpetian, Performance improvement of multi-DER microgrid for small- and large-signal disturbances and nonlinear loads: novel complementary control loop and fuzzy controller in a hierarchical droop-based control scheme, IEEE Syst. J. 12 (1) (2018) 444–451.
[20] I. Sadeghkhani, M.E.H. Golshan, A. Mehrizi-Sani, J.M. Guerrero, Low-voltage ride-through of a droop-based three-phase four-wire grid-connected microgrid, IET Gener. Transm. Distrib. 12 (8) (2018) 1906–1914.
[21] H. Bahramian-Habil, H.A. Abyaneh, G.B. Gharehpetian, Improving LVRT capability of microgrid by using bridge-type fault current limiter, Electr. Power Syst. Res. 191 (2021) 106872.
[22] X. Liu, et al., Fault current hierarchical limitation strategy for fault ride-through scheme of microgrid, IEEE Trans. Smart Grid 10 (6) (2019) 6566–6579.
[23] A. Camacho, M. Castilla, J. Miret, A. Borrell, L.G. De Vicuña, Active and reactive power strategies with peak current limitation for distributed generation inverters during unbalanced grid faults, IEEE Trans. Ind. Electron. 62 (3) (2015) 1515–1525.
[24] X. Guo, W. Liu, Z. Lu, Flexible power regulation and current-limited control of the grid-connected inverter under unbalanced grid voltage faults, IEEE Trans. Ind. Electron. 64 (9) (2017) 7425–7432.
[25] A. Camacho, M. Castilla, J. Miret, J.C. Vasquez, E. Alarcon-Gallo, Flexible voltage support control for three-phase distributed generation inverters under grid fault, IEEE Trans. Ind. Electron. 60 (4) (2013) 1429–1441.
[26] S. Ghosh, S. Chattopadhyay, Three-loop-based universal control architecture for decentralized operation of multiple inverters in an autonomous grid-interactive microgrid, IEEE Trans. Ind. Appl. 56 (2) (2020) 1966–1979.
[27] H.M. Hasanien, An adaptive control strategy for low voltage ride through capability enhancement of grid-connected photovoltaic power plants, IEEE Trans. Power Syst. 31 (4) (2016) 3230–3237.
[28] M.H. Syed, H.H. Zeineldin, M.S. El Moursi, Hybrid micro-grid operation characterisation based on stability and adherence to grid codes, IET Gener. Transm. Distrib. 8 (3) (2014) 563–572.
[29] R. Aboelsaud, A. Ibrahim, I.V. Aleksandrov, Z.M. Ali, Model predictive control algorithm for fault ride-through of stand-alone microgrid inverter, Int. J. Electr. Power Energy Syst. 135 (2022) 107485.
[30] M. Makhad, K. Zazi, M. Zazi, A. Loulijat, Adaptive super-twisting terminal sliding mode control and LVRT capability for switched reluctance generator based wind energy conversion system, Int. J. Electr. Power Energy Syst. 141 (2022) 108142.
[31] S. Roozbehani, M.T. Hagh, S.G. Zadeh, Frequency control of islanded wind-powered microgrid based on coordinated robust dynamic droop power sharing, IET Gener. Transm. Distrib. 13 (21) (2019) 4968–4977.
[32] N. Musarrat, A. Fekih, A fractional order sliding mode control-based topology to improve the transient stability of wind energy systems, Int. J. Electr. Power Energy Syst. 133 (2021) 107306.
[33] R.D. Kordkandi, M.T. Hagh, S. Roozbehani, Real-time low/high-voltage ride-through capability improvement of micro-grid based on coordinated robust grid-following control, IET Gener. Transm. Distrib. (2022) 1–15.
[34] N. Bouarroudj, D. Boukhetala, F. Boudjema, Sliding-mode controller based on fractional order calculus for a class of nonlinear systems, Int. J. Electr. Comput. Eng. 6 (5) (2016) 2239–2250.
[35] Institute of Electrical and Electronics Engineers, IEEE Std 1159 -IEEE Recommended Practice for Monitoring Electric Power Quality., vol. 2009, no. June. 2009, pp. 1-81. 10.1109/IEEESTD.2009.5154067.